Analytical 1D model of the flow-structure interaction in snoring

Filipe Soares, Jose Antunes, Vincent Debut, Christophe Vergez, Bruno Cochelin, Fabrice Silva

Analytical 1D model of the flow-structure interaction in snoring

Filipe Soares[*], Jose Antunes[*], Vincent Debut[**], Christophe Vergez[***], Bruno Cochelin[***] and Fabrice Silva[***]

** Instituto Superior Técnico – Centro de Ciências e Tecnologias Nucleares, Lisboa, Portugal*
*** Instituto Politécnico de Castelo Branco – Escola de Artes Aplicadas, Castelo Branco, Portugal*
**** Aix-Marseille Université, CRNS, Centrale Marseille, LMA UMR7031, Marseille, France*

Summary: The most common type of human snoring is characterized by vibrations of the soft-palate, induced by passing air during respiration. Despite being a widespread disorder, its occurrence is poorly understood and, consequently, clinical treatment is often ineffective. This physical system can be characterized, in its essence, by a cantilevered beam subjected to axial flow in a confined passage. These type of fluid-structure interaction systems have been a subject of research for many years, as its fundamental behavior is found in many other practical applications. Most studies are concerned solely with the conditions for linear stability and do not explore the ensuing nonlinear behavior of the system. This is particularly delicate as fluttering beams in confined flows are known to often result in dynamics with intermittent impacts between the beam and the side-walls. Here we present a nonlinear analytical resolution to a simplified 1-D model, based on a modal beam and bulk-flow equations. The model accounts for dissipation through distributed (frictional) and localized head-loss terms. The latter are imposed at the boundary conditions and aims to describe the complex effects occurring outside the domain (turbulence, vortex shedding, etc.). The present analytical resolution leads to a compact system for linear stability analysis, but also to a nonlinear formulation of the fluid-structure interaction. The inclusion of a regularized contact model allows for the computation of the full nonlinear dynamics, including intermittent impacts. Linear stability results are compared to previously published results using 2-D CFD models, and the relative merits of the model are discussed. A series of limit cycles with intermittent impacts between the beam and side-walls are presented to illustrate the nature of the post-instability oscillations. To the authors knowledge, the proposed formulation presents, for the first time, a framework for the comprehensive understanding of the nonlinear dynamics associated with flexible beams in confined axial flow.

Introduction

Recent studies suggest that no less than 30% of the adult population snores habitually. However, due its inherent complexity, the underlying physics and their relation to the type and degree of the disorder remain poorly understood and, consequently, treatment responses are often ineffective [1] [2]. The most common form of snoring is that of palatal snoring, where the vibration of the soft-palate/uvula (see Figure 1-(a)) is induced by the passage of air during respiration. This system can be categorized as a flow induced vibration problem. More specifically, it can be modelled as a flexible cantilever beam in confined axial flow [3] [4].

The static and dynamic instabilities associated with flexible beams/plates subject to axial flow occur also in different contexts from enhanced heat transfer [5], energy harvesting devices [6] or wind musical instruments [7]. The subject has been studied extensively [8], particularly for the case of unconfined flows. In these systems, the typical instability is of the flutter type. In the work of Shoele & Mittal [9], for example, we find some elucidating results regarding the influence of relevant non-dimensional parameters like the fluid-beam mass ratio, the reduced velocity (inverse of Strouhal number) or the confinement ratio (channel height to beam length ratio). Their results show that, at low beam-fluid mass ratios, the instability is of the single-mode flutter type, involving the coupling of the first two in-vacuo beam modes. As mass ratios increase, the initial single-mode flutter ceases to be the principal instability, and successive "mode-transitions" occur, whereby multiple higher-order fluttering modes prevail. This type of instability is commonly referred to as coupled-mode flutter.

More recently, the advances in computational efficiency have enabled the possibility to simulate these fluid-structure interaction (FSI) systems numerically by solving the Navier-Stokes equations in 2D and 3D domains [10]. These FSI models allow a more accurate representation of the physics. However, they also require considerable computational time, which becomes a handicap when analyzing problems whose behavior depends on a wide variety of parameters. For a more thorough parameter mapping, 1D models, based on simplified equations of motion, are not only computationally more efficient but also more tractable, and may provide valuable insights into the core dynamics of the problem.

In the context of simplified approaches, we note the work of Nagakura & Kaneko [11] that have used leakage flow theory to model the linear stability of a cantilever beam in a confined passage. Based on the work by Inada & Hayama [12], they formulate a 1D problem where flow pressure and velocity are taken as cross-sectionally averaged. The confinement is restricted to symmetric channels of constant cross-section, viscous effects are accounted for by a distributed friction term and the energy losses at the trailing edge are encapsulated by a localized head-loss term, imposed at the boundary condition.

By and large, the analytical models developed so far deal solely with the conditions for instability, using linearized equations of motions to study the effect of various parameters on the stability boundaries. Although undeniably a crucial information about the system dynamics, this gives us little insight about the ensuing nonlinear behavior. The

analysis of the nonlinear dynamics might by of valuable interest to various applications, giving information about human snoring, but also working regimes in wind musical instruments or in energy harvesting devices, for example.

In the context of unbounded flows, a number of theoretical and experimental studies can be found, illustrating the array of possible limit cycles arising in this type of systems [13] [14]. However, for instabilities in a confined passage, nonlinear modelling results and experimental observations have demonstrated the regular occurrence of limit cycles with intermittent impacts between the beam and the side walls [15] [16].

In this paper, we deal with a simplified 1D model in the spirit of Nagakura & Kaneko's work [11]. Contrary to their work, we admit channel profiles of any shape. More importantly however, we present an analytical resolution, based on formal solutions of the flow pressure and velocity fields, that leads not only to a compact system for linear stability analysis but also to a fully nonlinear flow formulation. This formulation can be used to explore post-instability regimes at very low computational costs. Additionally, to overcome the previously mentioned limitations, we add the possibility of contact between the flexible beam and the channel walls, enabling the calculation of limit-cycle oscillations (LCO) with, potentially, intermittent impacts.

Model Description

The model presented here deals with the fluid-structure interaction of a flexible beam confined by flow on each upper and lower sides, as illustrated in Figure 1. The formulation presented in the following is generic, in that it can, in principle, be applied to beams with arbitrary boundary conditions. However, in this paper we will deal solely with the particular case of a cantilever beam.

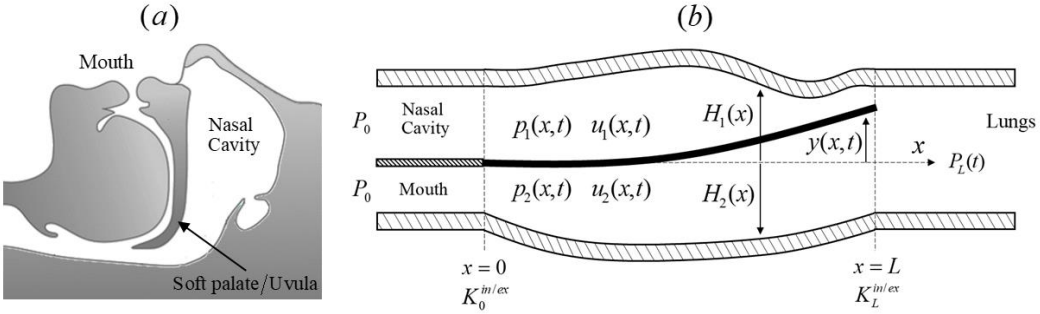

Figure 1 (a) Cross-sectional view of a human upper airway; (b) Schematic representation of the model.

Structural dynamics

The dynamics of a flexible linear beam are defined in terms of N modes, decoupled from the fluid. The modal parameters: modal masses m_n, frequencies ω_n, damping ratios ζ_n and mode shapes $\phi_n(x)$ can be calculated analytically for a beam with uniform cross-section or numerically for beams of any geometry, through either the Euler-Bernoulli or Timoshenko 1D linear beam equations. The beam displacement is developed as

$$y(x,t) = \sum_{n=1}^{N} \phi_n(x) q_n(t) \tag{1}$$

and the beam motion is finally described by the following set of N modal equations

$$m_n \ddot{q}_n(t) + 2m_n \omega_n \zeta_n \dot{q}_n(t) + m_n \omega_n^2 q_n(t) = b \int_0^L \left(p_2(x,t) - p_1(x,t) \right) \phi_n(x) dx \quad , \quad n = 1, 2 \ldots N \tag{2}$$

where b is the beam width and the modal forces are given by the projection of the pressure fields $p_1(x,t)$ and $p_2(x,t)$ (associated with the flow in the upper and lower channels, respectively), unto the beam modes.

Fluid dynamics

To derive the incompressible bulk-flow equations, we first consider small-to-moderate fluctuating channel heights $h_c(x,t)$, defined in terms of the beam motion

$$h_1(x,t) = H_1(x) - y(x,t) \qquad ; \qquad h_2(x,t) = H_2(x) + y(x,t) \tag{3}$$

where $H_1(x)$ and $H_2(x)$ are the distances from each wall to the position of the beam at rest and the index $c = 1,2$ corresponds to the upper and lower channels, respectively. Following the derivation by Antunes & Piteau [17], the flow variables are taken as cross-sectionally averaged, $p_c(x,t)$ and $u_c(x,t)$. The continuity and momentum equations of the fluid are given, respectively, for each channel $c = 1,2$, by

$$\frac{\partial h_c}{\partial t}+\frac{\partial}{\partial x}\left(h_c u_c\right)=0 \quad ; \quad \rho\left[\frac{\partial}{\partial t}\left(h_c u_c\right)+\frac{\partial}{\partial x}\left(h_c u_c^2\right)\right]+h_c\frac{\partial p_c}{\partial x}+\tau_c^w+\tau_c^b=0 \tag{4}$$

where ρ is the fluid's density, τ_c^w and τ_c^b are the shear stresses at the two interfaces (fluid-wall and fluid-beam) in each channel. Following the bulk-flow approach, the tangential stresses will be formulated as a head-loss model, given by

$$\tau_c^{w,b}=\frac{1}{2}\rho u_c\,|u_c|\,f_c^{w,b} \tag{5}$$

where f_c^w and f_c^b are the Fanning friction coefficients for each interface. Additionally, we assume both interfaces have equivalent frictional properties, hence $f_c^w=f_c^b=f$.

Aside from the distributed losses, we include as well singular dissipative effects at the boundaries. These are enforced at the boundary conditions and aim to encapsulate, in a simplified manner, the energy losses (turbulence, vortex shedding, etc.) occurring outside the domain. The second order system (4) is then submitted to the following flow boundary conditions at $x=0$ and $x=L$:

$$p_c(0,t)=P_0(t)-\rho\frac{1}{2}\left(u_c^2(0,t)-u_c(0,t)\left|u_c(0,t)\right|K_0\right) \;;\; p_c(L,t)=P_L(t)-\rho\frac{1}{2}\left(u_c^2(L,t)+u_c(L,t)\left|u_c(L,t)\right|K_L\right) \tag{6}$$

where K_0 and K_L are the singular head-loss coefficients at the boundaries; $P_0(t)$ and $P_L(t)$ are the imposed pressures. For the particular case of a cantilevered beam, the head-loss coefficient K_0 is bound to have a minimal effect on the dynamics, as it acts on the clamped end of the beam. For steady inflow (in the positive $x-$direction), it acts simply as a control-valve, limiting the flow energy entering the domain. On the other hand, the turbulent effects expected at the trailing-edge suggest that K_L will probably have a significant effect on the coupling dynamics. Following reference models [11] [18], we will take $K_L=1$ and $K_0=0$, which as shown to provide a reasonable representation in these types of FSI systems.

Nonlinear analytical approach using formal solutions

Integrating the continuity equation (4) with respect to x leads us to a formal solution for the velocity fields in each channel c:

$$u_c(x,t)=\frac{Q_c(t)-\int\dot{h}_c(x,t)dx}{h_c(x,t)} \tag{7}$$

where the "constants" of integration (actually, time domain functions) $Q_c(t)$ represent the global unsteady flow rates (per unit width) in each channel. After replacement of (7) in the momentum equation (4) and again integrating with respect to x, we obtain the formal solution for the pressure field in each channel,

$$p_c(x,t)=\rho\int\left(\begin{array}{c}\frac{\int\ddot{h}_c dx}{h_c}-2\frac{\dot{h}_c\int\dot{h}_c dx}{h_c^2}+\frac{h_c'\left(\int\dot{h}_c dx\right)^2}{h_c^3}-\frac{1}{h_c}\dot{Q}_c(t)+2\left(\frac{\dot{h}_c}{h_c^2}-\frac{h_c'\int\dot{h}_c dx}{h_c^3}\right)Q_c(t)\\ +\frac{h_c'}{h_c^3}Q_c(t)^2+f\left(\frac{\left(\int\dot{h}_c dx-Q_c(t)\right)\left|\int\dot{h}_c dx-Q_c(t)\right|}{h_c^3}\right)\end{array}\right)dx+S_c(t) \tag{8}$$

where spatial and temporal derivatives are denoted by an upper dash and dot, respectively. The new "constants" of integration $S_c(t)$ describe the pressure at the entrance of the channels $S_c(t)=p_c(0,t)$. From here on, to simplify notation, we define the following auxiliary variables describing the terms in the formal solutions

$$A_c(x,t)=-\frac{\int\dot{h}_c dx}{h_c} \;;\; B_c(x,t)=\frac{1}{h_c} \;;\; C_c(x,t)=\frac{\int\ddot{h}_c dx}{h_c}-2\frac{\dot{h}_c\int\dot{h}_c dx}{h_c^2}+\frac{\left(\int\dot{h}_c dx\right)^2}{h_c^3}\left(h_c'+f\,\mathrm{sign}\left(\int\dot{h}_c dx-Q_c(t)\right)\right);$$

$$D_c(x,t)=2\left(\frac{\dot{h}_c}{h_c^2}-\frac{\int\dot{h}_c dx}{h_c^3}\left(h_c'+f\,\mathrm{sign}\left(\int\dot{h}_c dx-Q_c(t)\right)\right)\right) \;;\; E_c(x,t)=\frac{1}{h_c^3}\left(h_c'+f\,\mathrm{sign}\left(\int\dot{h}_c dx-Q_c(t)\right)\right); \tag{9}$$

To enforce the boundary conditions, we replace the formal solutions (7)-(8) into expressions (6). After some algebra, we obtain two expressions for the constant of integration $S_c(t)$, in terms of $Q_c(t)$, $\dot{Q}_c(t)$ and the beam motion $A_c(x,t)-E_c(x,t)$. At the leading edge ($x=0$) we have simply

$$S_c(t) = P_0 - \rho\frac{1}{2}\left(1+\text{sign}\left(Q_c(t)\right)K_0\right)\left(B_c(0,t)Q_c(t)\right)^2 \tag{10}$$

while at the trailing edge ($x=L$) we get

$$S_c(t) = P_L(t) - \rho\left(\begin{array}{c} -\left(\int B_c(L,t)dx\right)\dot{Q}_c(t) \\ +\left(\int D_c(L,t)dx + A_c(L,t)B_c(L,t)\left[1-\text{sign}\left(A_c(L,t)+B_c(L,t)Q_c(t)\right)K_L\right]\right)Q_c(t) \\ +\left(\int E_c(L,t)dx + \frac{B_c^2(L,t)}{2}\left[1-\text{sign}\left(A_c(L,t)+B_c(L,t)Q_c(t)\right)K_L\right]\right)Q_c^2(t) \\ +\frac{A_c^2(L,t)}{2}\left[1-\text{sign}\left(A_c(L,t)+B_c(L,t)Q_c(t)\right)K_L\right]+\int C_c(L,t)dx \end{array}\right) \tag{11}$$

Then, combining (11) and (10), we are able to remove the constant of integration $S_c(t)$ and obtain two (one for each channel) first-order nonlinear ODEs in terms of the unsteady flow rates $Q_c(t)$,

$$\begin{array}{c} -\left(\int B_c(L,t)dx\right)\dot{Q}_c(t) \\ +\left(\int D_c(L,t)dx + A_c(L,t)B_c(L,t)\left[1-\text{sign}\left(A_c(L,t)+B_c(L,t)Q_c(t)\right)K_L\right]\right)Q_c(t) \\ +\left(\begin{array}{c}\int E_c(L,t)dx - \frac{B_c^2(0,t)}{2}\left(1+\text{sign}\left(Q_c(t)\right)K_0\right) \\ +\frac{B_c^2(L,t)}{2}\left[1-\text{sign}\left(A_c(L,t)+B_c(L,t)Q_c(t)\right)K_L\right]\end{array}\right)Q_c^2(t) \\ +\frac{A_c^2(L,t)}{2}\left[1-\text{sign}\left(A_c(L,t)+B_c(L,t)Q_c(t)\right)K_L\right]+\int C_c(L,t)dx + \frac{P_0(t)-P_L(t)}{\rho} = 0 \end{array} \tag{12}$$

Replacement of the formal solution for the pressure fields (8) into the beam modal equations (2), leads to a set of $2N$ nonlinear ODEs, in terms of the modal displacements $q_n(t)$, modal velocities $r_n(t)=\dot{q}_n(t)$ and the two unsteady flow rates $Q_1(t)$ and $Q_2(t)$. Together with the two flow rate ODEs (12), they form a closed set of first-order nonlinear differential equations describing the 1D fluid-structure model, in the form

$$[\mathbf{A}]\{\dot{\mathbf{x}}\}+[\mathbf{B}]\{\mathbf{x}\}=\{\mathbf{C}\} \tag{13}$$

where $\mathbf{x}=\{r_1(t),\dots r_N(t),\, q_1(t),\dots q_N(t),\, Q_1(t),\, Q_2(t)\}$, $[\mathbf{A}]$ and $[\mathbf{B}]$ are (dense) matrices of size $2N+2$, and $\{\mathbf{C}\}$ is a vector containing constant flow terms. Effectively, we are able to discretize our continuous 1D problem into a set of ODEs. However, there are nonlinear terms associated with beam motion (e.g. $\int A_c dx$) which contain modal summations in the denominator. As these terms cannot be simplified analytically, we do not reach "true" time-space separation, in the sense that the formulation does not contain time-independent spatial operators. During time-domain integrations, these terms need to be calculated at each time-step. Despite this fact, the formulation allows for temporal-integrations of the nonlinear system at very modest computational costs.

Results: linear stability and numerical validation

In this paper, for compactness, we have not shown the linearization of the above-mentioned system. It will suffice to say that linearization of the expressions above leads to a closed set of $2N+2$ ODEs (with constant spatial operators), which can then be formulated as an eigenvalue problem, from which we can infer the linear stability of the system under a set of given parameters.

In this section, with the aim of assessing the viability of the 1D simplified modelling approach and validating our results, we compare the linear stability results from our model to reference results. Even though the present modelling approach allows for channels of arbitrary shapes $H_c(x)$, we will consider only symmetric channels of constant section, i.e. $H_1(x)=H_2(x)=H$, on which most literature is based on. For the same reason, we will analyze configurations with flow in the positive direction only.

Following reference studies [9], we will present results in terms of the following non-dimensional parameters

$$U^* = U_0 L\sqrt{\frac{\rho_s e}{EI}} \quad ; \quad M^* = \frac{\rho_f L}{\rho_s e} \quad ; \quad H^* = \frac{H_0}{L} \tag{14}$$

where U^* is a reduced velocity (essentially the inverse of a Strouhal number), M^* is the fluid-beam mass ratio, and H^* is the confinement ratio. In our formulation, $H_0 = H_1(0) + H_2(0)$ and the fluid velocity U_0 is given by the steady component of the inlet velocity, i.e. $U_0 = (\bar{Q}_1 + \bar{Q}_2)/H_0$. Additionally, the Reynolds number Re is accounted implicitly by the Fanning friction coefficient f. To this end, we note the commonly used relation between Reynolds number Re and the friction coefficient f, established based on empirical data of steady flow [19], given by

$$\begin{cases} f = 12\,\mathrm{Re}^{-1} & \text{for} \quad \mathrm{Re} < \mathrm{Re}_0 \quad \text{(laminar)} \\ f = 0.055\,\mathrm{Re}^{-0.25} & \text{for} \quad \mathrm{Re} > \mathrm{Re}_0 \quad \text{(turbulent)} \end{cases} \tag{15}$$

where Re_0 is the Reynolds number separating laminar from turbulent flow ranges, taken here as $\mathrm{Re}_0 = 2500$.

Comparison to results from a 2-D viscous model

Here we compare linear stability results from our simplified model to those obtained by a more realistic 2D viscous model developed recently by Cisoni et al. [20]. In their paper [20], a 2D model is used to solve the nonlinear Navier-Stokes equations in the time-domain, including viscous effects. Several parametric sweeps were carried out to obtain stability curves in the nondimensional $(U^* - M^*)$ plane, for several (H^*, Re) pairings. Figure 2 shows a typical stability map in the $(U^* - M^*)$ plane, calculated with the present model and with the 2-D viscous model. Here, an undamped beam was considered, $\zeta_n = 0$, the confinement ratio was set at $H^* = 1/10$ and the Reynolds number at $\mathrm{Re} = 100$. Note that, in our formulation, the Reynolds number is set implicitly following relation (15), which leads to a friction coefficient $f \approx 0.14$. On the left are the stability boundaries in the $(U^* - M^*)$ plane and on the right the frequencies of the corresponding neutrally stable modes.

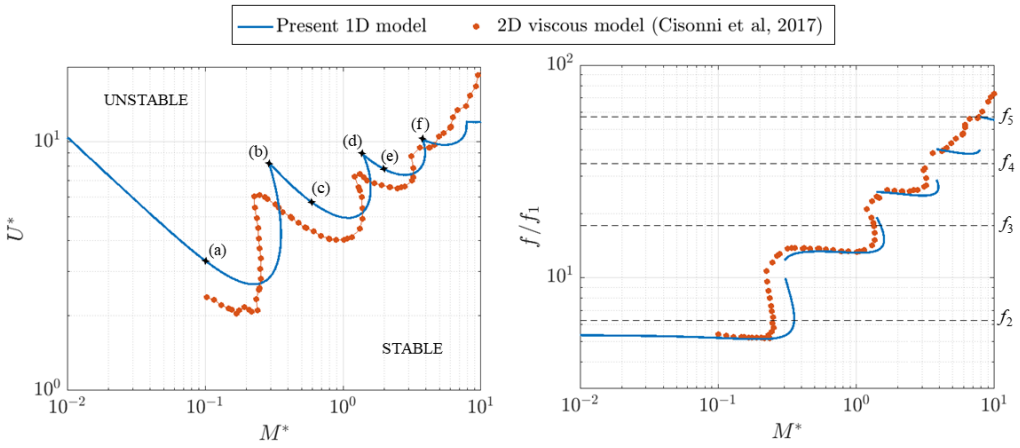

Figure 2 – Stability boundary in the $(U^* M^*)$ *plane (left) and the corresponding frequencies (right) for a system with confinement* $H^* = 1/10$ *and Reynolds number* $\mathrm{Re} = 100$. *The 2-D model results were retrieved from those presented in [20].*

The cascading stability boundary shown in Figure 2 is a typical result of cantilevered structures subject to axial flow, reported in many previous studies, including models which assume inviscid flow (see review in [9]). We note that results from the present model agree qualitatively well with those from the 2D model. Despite some minor quantitative differences, the overall stability behavior of the system is well encapsulated. Namely, the sharp transitions in the stability curves, associated with the well-known mode-switching behavior and illustrated clearly by the abrupt changes in the instability frequency, are well represented. This behavior occurs at increasing mass-ratios, whereby the first unstable mode in the system transitions from lower to higher order, i.e. the main unstable (coupled) mode is dominated by *in-vacuo* beam modes of progressively higher order. To clarify, Figure 3 illustrates the complex mode shapes associated with the various points (a)-(f) indicated in Figure 2. The minor quantitative differences (slight vertical and horizontal shifts in the $M^* - U^*$ plane), are likely explained by the inherent differences in the 1D and 2D modelling approaches, namely, the explicit vs. implicit account of viscous effects or the parabolic vs. constant velocity profiles stemming from explicit/implicit account of boundary layer effects.

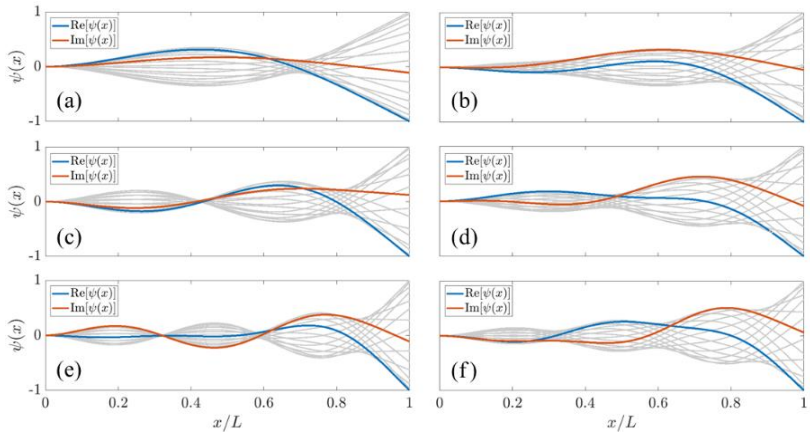

Figure 3 – Complex mode-shapes of the neutrally-stable modes associated with the boundary points (a)-(f) indicated in Figure 2. The real and imaginary parts of the mode shapes are indicated in blue and red, respectively. The grey lines illustrate the actual beam motion associated with the corresponding complex mode shapes.

Results: time-domain integrations and nonlinear dynamics

In this section we aim to explore the nature of the nonlinear regimes associated with a linearly unstable system through numerical time-domain integration. The set of nonlinear ODEs described in above (13) was solved using MATLAB's solver ode15i [21], an implicit scheme with variable time-stepping. Numerical simulations were started with the solutions of the steady configuration $\bar{q}_n$, $\bar{Q}_c$ as initial conditions, and a small perturbation force was applied to all beam modes to induce eventually unstable dynamics.

Stability and impact boundaries

As a first step to characterize the nonlinear behavior of the system, we examine the role of impacts and when they are more likely to occur. To this end, a series of numerical time-domain integrations were performed in the non-dimensional parametric space (U^*, M^*). We considered a symmetric configuration with confinement ratio $H^* = 1/10$, and friction coefficient $f = 0.14$. The simulations were run for several seconds until one of the following scenarios was encountered: (1) oscillations gradually decreased converging to the steady solution (linearly stable dynamics), (2) the oscillations grew until a stable limit cycle was reached, without the occurrence of impacts, or (3) oscillations grew until the beam eventually comes into contact with one of the walls, at which point the simulations were stopped. The difference between the latter two scenarios enabled us to estimate an "impact boundary", that is, a frontier in the (U^*, M^*) plane separating limit cycles with and without impacts. Because contact was not accounted in this first study, the beam was described by only $N = 10$ modes. All modal damping coefficients were set to $\zeta_n = 0.01$. The resulting map is shown in Figure 4.

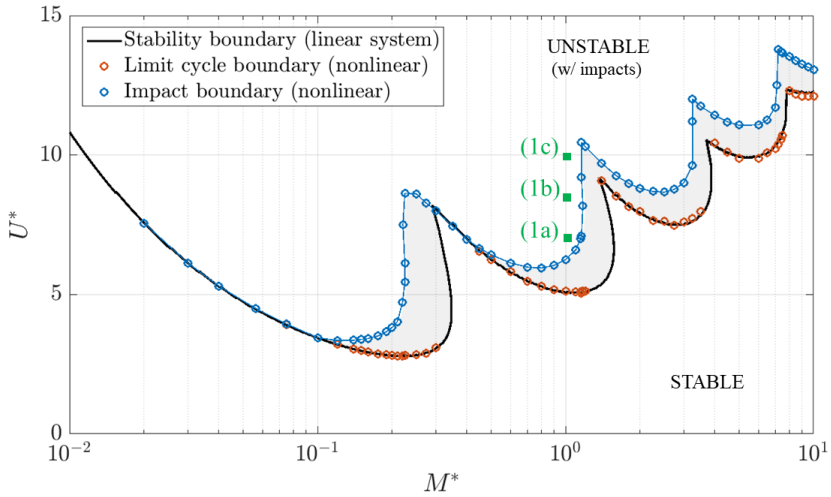

Figure 4 – Stability map of a system with confinement ratio $H^* = 1/10$ and friction coefficient $f = 0.14$, in the (U^*, M^*) plane. The linear stability boundary (black line) is compared to the limit cycle boundary found by the nonlinear simulations (orange circles). The impact boundary (blue line) illustrates the frontier in which unstable dynamics lead to contact between the beam and the confinement walls. The nonlinear limit cycles associated with the points marked (1a-c) will be shown in the following sections.

We see that the stability boundary predicted by the linearized system is coherent with the unstable dynamics observed in the nonlinear simulations. As for the impact boundary, we note that the regions in which limit cycles without impacts occur (grey area) are not extensive. Noticeably, we underline the fact that for small mass ratios (heavy beams or light fluids) these regions simply do not exist and the flutter instability, however weak, inevitably leads to large amplitude beam motions and eventual contact with the side walls. This seems physically plausible as, in these cases, the inertia of heavier beams will tend to outweigh the restoring forces from a light fluid.

Elastic impact model

Numerous experimental (and modelling) observations [3] [4] [14] [16] demonstrate that nonlinear motions of cantilevered plates in confined axial flow regularly present intermittent impacts between the beam and the side-walls. Consequently, previous attempts at modelling limit-cycle oscillations (LCO), eventually encountered limitations in their solutions, at regimes where the motion of the plate is large enough that collisions become inevitable.

In the current bulk-flow formulation, the addition of dynamic impact between the beam and the side walls is not a trivial task. One of the major challenges relates to the fact that the solutions for flow velocity and pressure fields present singularities at the moment of contact, i.e. when the channel height $h_c = 0$. Consequently, classical penalty methods, reliant on "interpenetration", are incompatible with the current flow model. Without dealing with these delicate issues, here we present a pragmatic approach, based on a regularized impact formulation, that allows us to include impacts in a simple manner that is compatible with the flow formulation. Since the fluid equations do not allow for beam penetration, an impact force $F_i(x,t)$ is applied on the beam just before contact, in regions of the beam which have trespassed a small regularization parameter ε (Figure 5). In essence, we allow some flow leakage at the moments of "contact", such that an impact force can be applied to the beam without fully restricting the flow dynamics.

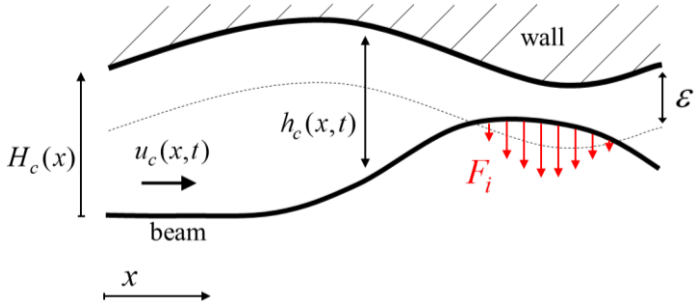

Figure 5 – Illustration of the beam violation right before contact and corresponding impact force.

A simplified version of a classic Hertz model is considered, where the impact force is linearly proportional to a violation parameter $v(x,t)$, describing the penetration distance between the beam a "virtual" wall defined by $H_c(x) - \varepsilon$, as illustrated in Figure 5. Then, the impact force $F_i(x,t)$ is given by

$$F_i(x,t) = \begin{cases} k_i\, v(x,t) & \text{if } v(x,t) > 0 \\ 0 & \text{otherwise} \end{cases} \tag{16}$$

where k_i is an impact stiffness and the violation amplitude is given by $v(x,t) = \varepsilon - h_c(x,t)$. The sign of $F_i(x,t)$ is defined for each channel: $F_i > 0$ for $c = 2$; $F_i < 0$ for $c = 1$.

Illustrative examples of limit-cycle oscillations with intermittent impacts

Here we illustrate a few limit cycles that include intermittent impacts, namely, the solutions for the configurations indicated in Figure 4 by points (1a), (1b) and (1c). These configurations have a constant mass ratio of $M^* = 1$ and various reduced velocities $U^* = [7, \ 8.5, \ 10]$, respectively. For these simulations, a large number of beam modes was considered, $N = 40$, to ensure the impact dynamics are well represented. In the following simulations, the non-dimensional impact stiffness was taken as $k_i^* = k_i / m_1 \omega_1^2 = 10^6$ (normalized by the stiffness of the first beam mode) and the non-dimensional regularization parameter $\varepsilon / H = 10^{-3}$.

Figure 6 shows snapshots of the beam motion and Figure 7 the evolution of the modal velocities $r_n(t)$ and the unsteady flow rates $Q_c(t)$, for the three configurations (1a), (1b) and (1c). Moreover, in Figure 8 we show the phase-portrait of the beam tip, the evolution of the tip displacement $y(L,t)$, the spectra of the tip velocity and RMS-value of the modal displacements $q_n(t)$, for all three configurations. Finally, we show in Figure 9 the impact force applied on the beam throughout the limit cycles. The impact force is expressed as the spatial integral of $F_i(x,t)$, normalized by a reference force $F_0 = m f_1^2 H$, where m is the total mass of the beam and f_1 is the frequency of the first in-vacuo beam mode.

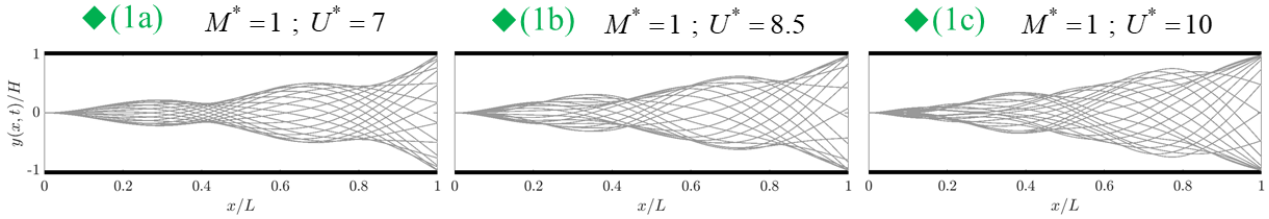

Figure 6 - Snapshots of the beam motion during one cycle for configurations (1a), (1b) and (1c).

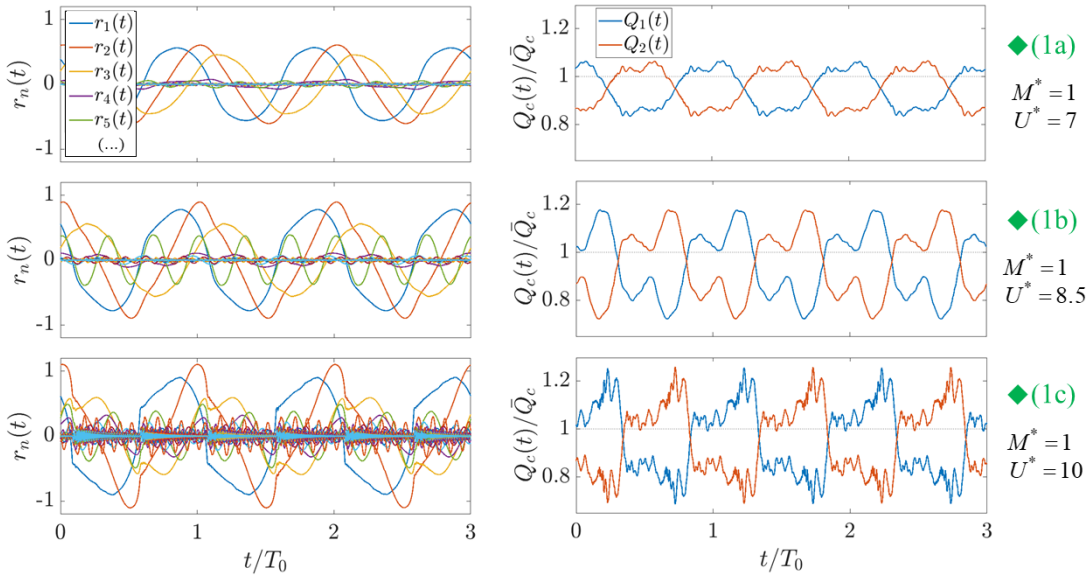

Figure 7 - Temporal evolution of the modal velocities $r_n(t)$ (left) and unsteady flow rates $Q_c(t)$ (right) in the limit cycles associated with configurations (1a), (1b) and (1c). For clarity, time scales are normalized by the fundamental period of the corresponding limit-cycle T_0.

In Figure 6 we notice that, in all cases, intermittent contact occurs solely at the tip of the beam. As the velocity U^* increases (1b-c), impacts become more violent and the beam motion becomes increasingly perturbed, as higher order beam modes are intermittently excited and start playing a more prominent role in the overall beam motion. These effects are also seen by the evolution of the modal velocities shown in Figure 7 and the RMS-values in Figure 8 . When impacts are relatively weak (1a), the tip simply "grazes" the wall and the overall beam motion is not significantly altered compared to the mode shapes estimated by the linear stability analysis.

Similarly, the oscillations of the flow rates become increasingly abrupt in the presence of violent impacts. However, it is interesting to note that sharp changes in the unsteady flow-rate (e.g. bottom-right plot in Figure 7) do not occur at the moments of contact but rather at the moments when the beam motion rapidly shifts from one side of the channel to the other. This effect can be illustrated, for example, by the beam-tip motion shown in Figure 8. Here we notice that as impacts become stronger, the overall contact time also becomes larger, meaning as well that the beam-tip will shift sides more abruptly, hence generating sharp fluctuations in the flow-rates. As expected, flow rates also oscillate around a value slightly lower than their steady component $\bar{Q}_c$. This means that the overall mass transport is reduced by the fluttering beam, compared to a static scenario. This seems physically plausible as, during flutter, some of the energy carried by the flow is transferred to the beam and lost through either structural dissipation or increased flow-dissipation effects.

In Figure 8 we note that the motions become increasingly nonlinear in the presence of stronger impacts. The phase-portrait shows more perturbed motions with larger gradients. Naturally, the spectra of the beam tip show a large number of high order harmonic components, increasing in amplitude as impacts become more violent. It is worth noting that, in limit cycles with very strong impacts (1c), the oscillations are not strictly periodic. Although the low frequency motions are stable, we notice small high frequency perturbations, related to the unsynchronized motion of the intermittently excited higher order beam modes. This behavior is clearly illustrated by the spectra of (1c), where we notice not only an increase in the amplitude of the harmonics, but also a visible presence of noise-like spectral behavior. Nevertheless, these motions might be tentatively classified as perturbed periodic oscillations, rather than aperiodic dynamics.

The impact forces represented in Figure 9 illustrate the fact that, during each beam-wall interaction, the beam tip impacts the wall multiple times. This chattering effect is a typical behavior of systems with impacts in multi-modal structures. In weaker impacts (1a) we notice only a few impacts of decreasing strength while in more violent regimes (1b-c) contact is composed of multiple impacts with stronger associated forces and an overall longer chattering time.

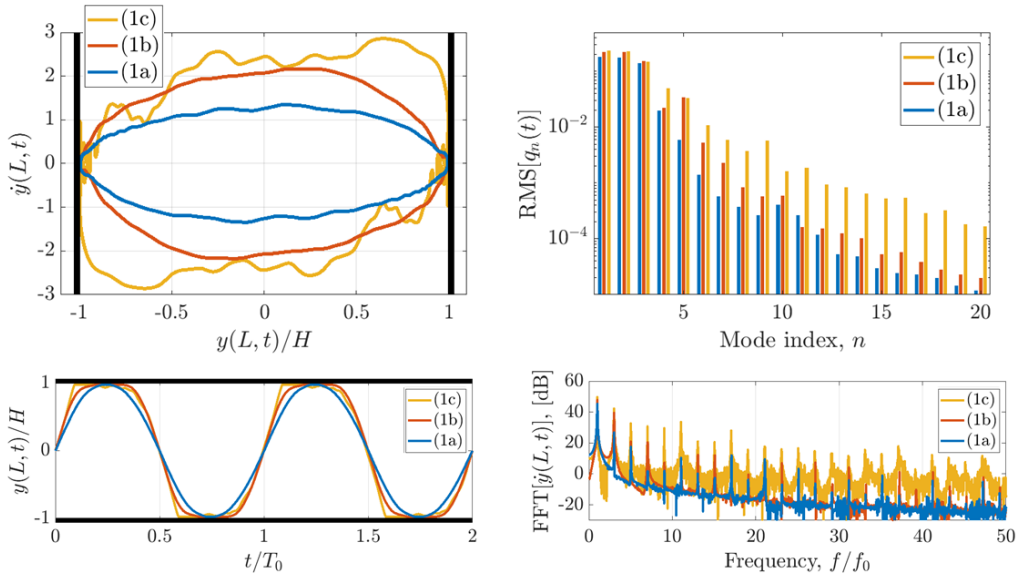

Figure 8 - Phase-portrait of beam tip (top-left); root-mean-square (RMS) value of the modal displacements (top-right); beam tip displacement (bottom-left) and spectra of the tip velocity (bottom-right, for the three configurations (1a), (1b) and (1c). For clarity, time/frequency scales are normalized by the fundamental period/frequency of the corresponding limit-cycle T_0 *and* f_0.

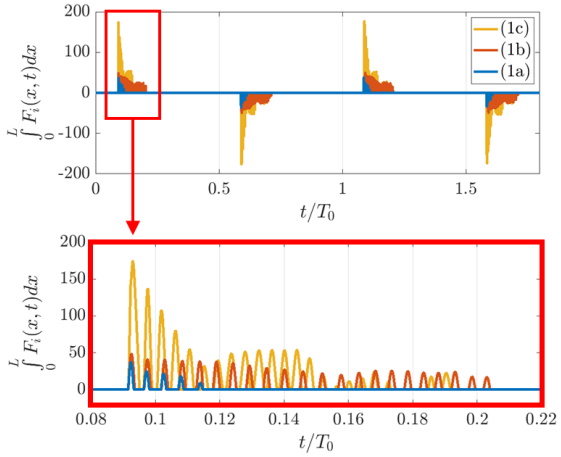

Figure 9 – The evolution of the non-dimensional impact force through the limit-cycles associated with configurations (1a), (1b) and (1c). For clarity, time scales are normalized by the fundamental period of the corresponding limit cycle T_0.

Conclusions

In this paper we have presented a framework for the comprehensive study of the nonlinear dynamics of a flexible beam subject to axial flow in a confined passage. Previous studies have been constrained by either large computational costs associated with 2D CFD models, the lack of a nonlinear flow formulation, and/or by the occurrence of contact between the beam and the side-walls. Here, a 1D model was formulated where the beam is described by its in-vacuo modes and incompressible bulk-flow equations, including distributed and localized head-losses, are used for the flow in both channels. An analytical resolution, based on the formal solutions for the velocity and pressure fields, is developed and leads to a fully nonlinear formulation of the fluid-structure interaction. Moreover, the possibility of contact between the beam and the walls is accounted for by a regularized impact model.

As a preliminary assessment of the potential of the proposed approach, results of linear stability analysis were compared to reference results using more realistic 2D CFD model. Overall, results were positively validated with only minor quantitative differences, at least for relatively narrow passages. Although not shown here, for brevity, it is worth noting that for larger confinement ratios $H/L >\sim 1/5$, we notice larger errors, as expected from the simplifying assumptions made in the bulk-flow approach.

Subsequently, nonlinear time-domain integrations were performed in order to illustrate the dynamical behavior occurring in such systems. Firstly, several simulations were performed to characterize the nonlinear dynamics for different configurations in the (M^*, U^*)-space. This led to a mapping of the nonlinear dynamics, separating the regions where limit cycles with and without impacts occur. Results suggest that, for low mass ratios (heavy beams/light fluids), the initial flutter instability always leads to contact, likely due to the contrast of the inertia of a heavy beam to that of a

light fluid. For moderate-to-large mass ratios, there are regions in the (M^*, U^*)-space where limit cycles without impacts occur, although these are relatively narrow. Secondly, several LCO with intermittent impacts were shown to elucidate the nature of the resulting nonlinear regimes. The lack of experimental data on the ensuing limit-cycles prevents us from a meaningful validation of our results, nevertheless, they seem physically plausible and consistent with experimental observations, at least qualitatively.

To the authors best knowledge, the presented framework allowed, for the first time, the calculations of the post-instability behavior of fluttering beams in confined flow, including vibro-impact dynamics. Future work might deal with the refinement of the impact model, to treat flow contact conditions and include damping. Moreover, bifurcation analysis using methods for the calculation and continuation of periodic solutions can contribute to a more comprehensive understanding of the associated nonlinear dynamics.

References

[1] A. T, V. A and P. O, "Understanding sleep-disordered breathing through mathematical modelling," *Sleep Medical Reviview,* vol. 13, no. 5, pp. 333-343 , 2009.

[2] P. Norton and E. Dunn, "Snoring as a risk factor for disease: an epidemiological survey," 1995.

[3] Y. Aurégan and C. Depollier, "Snoring: Linear Stability Analysis and In-Vitro Experiments," *Journal of Sound and Vibration,* vol. 188, no. 1, pp. 39-54, 1995.

[4] L. Huang, "Mechanical Modeling of Palatal Snoring," *Journal of the Acoustical Society of America,* vol. 97, pp. 3642-3648, 1995.

[5] P. Hidalgo, S. Jha and A. Glezer, "Enhanced heat transfer in air cooled heat sinks using aeroelastically fluttering reeds," *Thermal Investigations of ICs and Systems (THERMINIC),* pp. 1-6, 2015.

[6] S. Sherrit, H. Lee, P. Walkemeyer, T. Winn, L. Tosi and T. Colonius, "Fluid flow nozzle energy harvesters," *Sensors and Smart Structures Technologies for Civil, Mechanical, and Aerospace Systems,* 2015.

[7] F. Avanzini and M. Walstijn, "Modelling the mechanical response of the reed-mouthpiece-lip system of a clarinet. Part 1: a one-dimensional distributed model," *Acta Acustica United with Acustica,* vol. 90, pp. 537-547, 2004.

[8] M. P. Paidoussis, Fluid-Structure Interactions: Slender Structures and Axial Flow, San Diego, California: Academic Press, 2004.

[9] K. Shoele and R. Mittal, "Flutter instability of a thin flexible plate in a channel," *Journal of Fluid Mechanics,* vol. 786, pp. 29-46, 2016.

[10] G. Tetlow and A. Lucey, "Motions of a cantilevered flexible plate in viscous channel flow driven by a constant pressure drop," *Communications in Numerical Methods in Engineering,* 2009.

[11] H. Nagakura and S. Kaneko, "Stability of a cantiliver beam subject to one-dimensional leakage flow," *Proceedings Asia-Pacific Conference '93, Kitakyushiu, Japan,* vol. 1, pp. 352-359, 1993.

[12] F. Inada and S. Hayama, "A Study on the Leakage-Flow-Induced Vibrations. Part 1: Fluid Dynamic Forces and Moments Acting on the Walls of a Narrow Tapered Passage," *Journal of Fluids and Structures,* vol. 4, pp. 395-412, 1990.

[13] Y. Yadykin, V. Tenetov and D. Levin, "The flow induced vibration of a flexible strip hanging vertically in parallel flow. Part 1: temporal aeroelastic instability," *Journal of Fluids and Structures,* vol. 15, pp. 1167-1185, 2001.

[14] S. Alben, "Flag flutter in inviscid channel flow," *Physics of Fluids,* vol. 27, 2015.

[15] X. Wu and S. Kaneko, "Linear and Nonlinear analyses of sheet flutter induced by leakage flow," *Journal of Fluids and Structures,* vol. 20, pp. 927-948, 2005.

[16] K. Fujita, H. Morikazu and A. Shintani, "A consideration on pre- and post-instability of an axisymmetric elastic beam subject to axil leakage flow," *Journal of Fluids and Structures,* vol. 23, pp. 463-478, 2007.

[17] J. Antunes and P. Piteau, "A nonlinear analytical model for the squeeze-film dynamics of parallel plates subject to axial flow," *Journal of Fluids and Structures,* vol. 52, pp. 1491-1504, 2010.

[18] L. P. Tosi and T. Colonious, "Modelling and simulation of a fluttering cantilever in channel flow," *Journal of Fluids and Structures,* 2019.

[19] R. Blevins, Fluid Dynamics, New York, USA: Van Nostrand Reinhold Company, 1984.

[20] J. Cisonni, A. Lucey, N. Elliot and M. Heil, "The stability of a flexible cantilever in viscous channel flow," *Journal of Sound and Vibration,* 2017.

[21] "MATLAB - Numerical Integration and Differential Equations," Mathworks, Inc., 2021. [Online]. Available: https://www.mathworks.com/help/matlab/ref/ode15i.html.